

The composition of Mars' topside ionosphere: Effects of hydrogen

Majd Matta,¹ Paul Withers,¹ and Michael Mendillo¹

Received 3 August 2012; revised 18 December 2012; accepted 23 December 2012; published 24 May 2013.

[1] A one-dimensional model of the Martian ionosphere is used to explore the importance of atomic and molecular hydrogen chemistry in the upper atmosphere and ionosphere. Neutral and ionized H and H₂ undergo chemical reactions that lead to the production of the hydrogenated ions: H⁺, H₂⁺, H₃⁺, OH⁺, HCO⁺, ArH⁺, N₂H⁺, HCO₂⁺, and HOC⁺. Simulations are conducted for the cases of photochemistry only and photochemistry coupled with transport in order to assess the separate effects of plasma diffusion in the topside ionosphere. For both of these cases, the sensitivity of the ionosphere is tested for (1) molecular hydrogen abundance and (2) reaction rate, k_1 , for the charge exchange between H⁺ and H₂. Results are reported for midday solar minimum conditions. We find that the ionospheric composition of Mars is sensitive to H₂ abundance, but relatively insensitive to the reaction rate, k_1 . Depending on the conditions simulated, the topside ionosphere can contain appreciable amounts of hydrogenated species such as H₃⁺, OH⁺, and HCO⁺. Comparisons are made with Viking ion density measurements as well as with results of other published Mars ionospheric models. Future comparisons with more extensive ion composition will be available when the Mars Atmosphere and Volatile Evolution mission arrives at Mars.

Citation: Matta, M., P. Withers, and M. Mendillo (2013), The composition of Mars' topside ionosphere: Effects of hydrogen, *J. Geophys. Res. Space Physics*, 118, 2681–2693, doi:10.1002/jgra.50104

1. Introduction

[2] The composition of the ionized component of a planet's atmosphere is dependent on the composition of its neutral counterpart. The atmospheric composition of Mars has been measured remotely and in situ with too little frequency to result in any definitive global map of the major and minor constituents. Hence, measurements from various instruments and spacecraft are often pooled to provide a representative picture of the neutral atmosphere.

[3] Early efforts of remotely measuring the Martian upper atmosphere revealed CO₂, H₂O, and CO [Kuiper, 1952; Kaplan *et al.*, 1964, 1969; Young and Young 1977]. While Mariner 4 quantified the total pressure at Mars [Kliore *et al.*, 1965], Mariners 6, 7, and 9 and Mars-3 took in situ spectra that quantified the abundance of H, CO, and O at ~220 km [Anderson and Hord, 1971, 1972; Barth *et al.*, 1971, 1972; Dementyeva *et al.*, 1972; Strickland *et al.*, 1972; Anderson, 1974; Moos, 1974]. A few decades after the first flyby of Mars, remote sensing of atomic hydrogen Lyman- α emissions was made by the Hubble Space Telescope and the Far Ultraviolet Spectroscopic Explorer (FUSE). The resulting measurements quantified H and H₂ abundances in the Martian atmosphere [Krasnopolsky, 2000, 1998; Krasnopolsky and Feldman, 2001]. More recently,

the Mars Express (MEX) mission made spectral measurements of H and O at 200 km using the Spectroscopy for Investigation of Characteristics of the Atmosphere of Mars instrument [Bertaux, 2000; Chaufray *et al.*, 2007, 2008, 2009; Valeille *et al.*, 2009] and the Analyzer of Space Plasma and Energetic Atoms instrument [Galli *et al.*, 2006]. Furthermore, the Rosetta flyby of Mars during a gravity assist maneuver made spectral detections of H and O at exospheric altitudes [Feldman *et al.*, 2011].

[4] To date, the Viking 1 and 2 Landers mark the only spacecraft to successfully deliver in situ measurements of the atmosphere and ion composition of Mars between 120 and 200 km [Nier and McElroy, 1976]. Viking neutral mass spectrometers measured abundances of major species, CO₂, N₂, Ar, CO, O₂, and NO, and analyzed upper limits of mixing ratios of minor species such as H₂ and He. Atomic oxygen was also detected as a major neutral species, but quantitative in situ measurements could not be made due to contamination of the instrument by terrestrial sources [Nier *et al.*, 1976; Nier and McElroy, 1976; Nier and McElroy, 1977]. The Viking Landers also measured ion density profiles of O⁺, CO₂⁺, and O⁺ [Hanson *et al.*, 1977].

[5] Preceding the H₂ measurements at Mars mentioned above, ionospheric simulations neglected to include minor atomic and molecular hydrogen species [e.g., Hanson *et al.*, 1977; Kong and McElroy, 1977; McElroy *et al.*, 1977; Chen *et al.*, 1978; Fox and Dalgarno, 1979; Singh and Prasad, 1983; Krasnopolsky, 1993a, 1993b; Nair *et al.*, 1994; Krasnopolsky, 1995; Fox *et al.*, 1996]. FUSE measurements of Martian H₂ revealed its dominance in the neutral atmosphere above 250 km [Krasnopolsky *et al.*, 1998]. Since molecular hydrogen is chemically reactive with its surrounding ions, it can have major effects on the composition of the ionosphere.

¹Department of Astronomy, Boston University, Boston, Massachusetts, USA.

Corresponding author: M. Matta, Department of Astronomy, Boston University, Boston, MA 02215, USA. (majdm@bu.edu)

[6] The H_2 mixing ratio was determined with some uncertainty to vary between 20 and 50 ppm at 80 km [Krasnopolsky *et al.*, 1998; Krasnopolsky and Feldman, 2001; Krasnopolsky, 2002, 2003; Fox and Yeager, 2009]. Fox and Bakalian [2001] were among the first to address the quantitative effects of H_2 on the Martian atmosphere. They found that H_2 would affect the secondary ion chemistry of N_2H^+ , OH^+ , HCO^+ , and HCO_2^+ , and they concluded that the adopted mixing ratio of 40 ppm was too large. A follow-up study by Fox [2003] showed the effects of varying the abundance of H_2 on O^+ , CO_2^+ , N_2^+ , and CO^+ . In an effort to improve agreement of modeled O^+ densities with those measured by Viking below 200 km, the mixing ratio of H_2 was varied from 4, 10, 15, 40 to 100 ppm. Due to the high reactivity of H_2 with O^+ , it was found that the lower the mixing ratio and the higher the modeled O^+ density, the better is the match between models and Viking measurements. However, there has been relatively little follow-up on the importance of hydrogen on ion composition [Krasnopolsky, 2002; Fox, 2004a, 2004b, 2005; Fox and Yeager, 2006, 2009; Fox and Hać, 2009]. No study to date has explored systematically the effects of H and H_2 chemistry on the upper ionosphere of Mars.

[7] The objective of this work is to analyze the combined effects of atomic and molecular hydrogen chemistry at Mars, with particular attention to the topside ionosphere. Section 2 describes the model customized to include atomic and molecular hydrogen chemistry for use in this work. Section 3 shows the main results of the simulations using two sensitivity experiments. In Section 4, the model results are compared with measurements and other models and then discussed. Conclusions are drawn in Section 5.

2. Model Description

[8] Planetary atmospheric and ionospheric models are abundant for Mars [Bougher *et al.*, 2008; González-Galindo *et al.*, 2011; Haider *et al.*, 2011]. One-dimensional (1-D) models represent simplified yet quantitative tools for gaining insight to the major neutral and ionized constituents of an atmosphere, as well as to the physical processes controlling those regions. An existing 1-D model has been adapted for this study. This model was first used to analyze the variability in the photochemical regions of the Martian ionosphere [Martinis *et al.*, 2003]. The model was later upgraded to include plasma diffusion and was used for a study of simultaneous Mars Global Surveyor (MGS) and MEX radio occultation data sets, and to simulate and analyze the effects of flares on the ionosphere at Mars [Mendillo *et al.*, 2011; Lollo *et al.*, 2012].

[9] The simulations of this work are conducted for the same conditions used by Mendillo *et al.* [2011] for the MGS dataset: solar minimum conditions ($F_{10.7} \sim 84$), a Mars-Sun distance of 1.5943 AU, solar declination of 19.8° , latitude of 66.7° north, at summer solstice with a resulting SZA $\sim 47^\circ$ at local noon. The model is run for 2 sols (Martian days), and results from the second day's run at local noon are shown.

[10] A detailed description of the model can be found in Mendillo *et al.* [2011]. To summarize, this model simulates the Martian ionosphere between 80 and 400 km and takes as input (1) a neutral atmosphere consisting of CO_2 , O, N_2 , CO, and H_2 as described by version 4 of the Mars Climate

Database (MCD) [Forget *et al.*, 1999; Lewis *et al.* 1999], (2) an exospheric neutral temperature from the MCD, (3) absorption and ionization cross sections from Verner and Yakovlev [1995] and Verner *et al.* [1996] for wavelengths 1.86–4.92 nm and from Schunk and Nagy [2009] for wavelengths 5.05–105 nm, and (4) solar irradiance for wavelengths 1.86–105 nm from Solar2000 [Tobiska, 2004] that is scaled to Mars' location. Empirical representations of secondary ionization yield and plasma temperatures were developed from the parameterizations based upon the detailed calculations of Fox *et al.* [1996] and Nicholson *et al.* [2009]. The secondary ionization ratio varies smoothly from 0.3 in the upper boundary to 11 in the lower boundary. These representations were optimized via constraints by MGS and MEX radio occultation profiles [Mendillo *et al.*, 2011].

[11] The model solves equations for generating a neutral atmosphere between 80 and 400 km based on mixing ratios at 80 km that propagate neutral species concentrations upwards via molecular and eddy diffusion [Krasnopolsky, 2002]. The volume mixing ratios supplied by the MCD are more reliable at lower altitudes. The resulting neutral atmosphere that is derived compares well with Viking Lander measurements for overlapping species at overlapping altitudes. Five ions are generated via photo-ionization and photochemistry: O_2^+ , O^+ , CO_2^+ , N_2^+ , and NO^+ . The coupled continuity and momentum equations are then solved along the vertical dimension using solar production, chemical production and loss, and vertical transport with ion-neutral collisions to obtain ion densities and velocities as a function of time. The model time steps are orders of magnitude smaller than photochemical and transport timescales. Solar wind effects upon the ionospheric plasma are not in the model; i. e., it is assumed that the solar wind plasma lies above the top altitude boundary of 400 km. However, the altitude of the region separating solar wind from planetary plasma at Mars is not well defined and could be lower than the model's upper boundary altitude [Mitchell *et al.*, 2001; Withers, 2009], and so the results of this work are summarized for ion composition at 250 km, 300 km and 350 km.

[12] A similar modeling approach to the one used here was applied to Saturn's ionosphere. The Saturn model uses the same numerical techniques for plasma transport as used for Mars and has been validated using Cassini electron density profiles, as well as checked for consistency using a 3-D general circulation model [Moore *et al.*, 2004; Müller-Wodarg *et al.*, 2006; Moore and Mendillo, 2007; Moore *et al.*, 2010, 2012].

2.1. Updates to the Neutral Atmosphere

[13] The same neutral atmosphere derived from the MCD (version 4.3) and used in Mendillo *et al.* [2011] was used for this work with some additions. The MCD is an online resource of Martian atmospheric parameters derived from a 3-D general circulation model. The MCD is a collaborative effort developed at the Laboratoire de Meteorologie Dynamique du CNRS (Paris, France), Open University (UK), Oxford University (UK), and the Instituto de Astrofísica de Andalucía (Spain). The parameters available for lookup in the model are neutral density, pressure, temperature, and turbulent kinetic energy; surface temperature, pressure, and CO_2 ice layer; volume mixing ratios of CO_2 , CO, H_2 , O, N_2 , H_2O ice, and H_2O vapor; 3-D neutral wind components;

water ice and vapor columns; solar and thermal radiative fluxes and dust optical depth. The 3-D MCD offers these parameters as a function of dust scenario, latitude, longitude, local time, and altitude ranging from the surface up to 230 km [Forget *et al.*, 1999; Lewis *et al.* 1999; Angelats *i Coll et al.*, 2005; González-Galindo *et al.*, 2005; Millour *et al.*, 2011]. The database is readily available for reference at <http://www-mars.lmd.jussieu.fr/>. The MCD is validated with measurements from MGS Thermal Emission Spectrometer for surface temperature, atmospheric temperature, and water vapor column; radio occultation measurements using the ultra-stable oscillator on MGS for atmospheric temperature; and Viking Landers and Pathfinder for surface pressure.

[14] The 1-D model of Mendillo *et al.* [2011], and this work, used MCD-provided mixing ratios of CO₂, O, N₂, CO, and H₂ to generate a neutral atmosphere. The resulting CO₂, O, N₂, and CO profiles agree with the density profiles measured by the Viking Landers. H₂ densities are more challenging to validate as there are no in situ measurements to compare with. FUSE detections of Martian H₂ from mostly Lyman-β photons gave a mixing ratio for H₂ of 15 ± 5 ppm and a corresponding density of 10⁵ cm⁻³ at ~220 km for solar maximum conditions [Krasnopolsky and Feldman, 2001]. Densities of molecular hydrogen at 250 km were modeled to be ~2–50 × 10⁵ cm⁻³ (T_∞ ~ 200 K) and ~1–5 × 10⁵ cm⁻³ (T_∞ = 350 K) for solar minimum and maximum conditions, respectively, where T_∞ is the exospheric temperature [McElroy *et al.*, 1977; Krasnopolsky, 2000, 1998; Krasnopolsky and Feldman, 2001; Fox, 2003]. For solar minimum conditions, there is about an order of magnitude difference in the limits of estimated neutral molecular hydrogen in the Martian atmosphere. Presently, H₂ mixing ratios in the MCD are still under development [F. Forget, 2011, personal communication]. At 80 km, MCD provides 16 ppm of molecular hydrogen that results in a concentration of 3 × 10⁶ cm⁻³ at 200 km (for T_∞ = 205 K), close to the upper limit given by other models. The molecular hydrogen mixing ratio in this model is therefore treated as a free parameter with densities at 200 km ranging between 10⁵ and 10⁶ cm⁻³. This corresponds to a mixing ratio of 1.6 and 16 ppm at 80 km.

[15] To the MCD mixing ratios, two more neutral species, H and Ar, have been added to expand the ion-neutral chemistry in this work. An atomic hydrogen neutral density profile was added by incorporating a volume mixing ratio at 80 km for H and then using the existing formulae to generate concentrations as a function of altitude up to 400 km. Since there are no in situ measurements of atomic hydrogen at Mars, the H neutral density at ~220 km is constrained to match Lyman-α airglow measurements made by spacecraft. A summary of such measurements is reviewed in Table 1. The density of H at 220 km during the solar minimum conditions modeled here is ~2 × 10⁵ cm⁻³. At higher altitudes, the extrapolated density for H compares well with those of other models for similar conditions [Krasnopolsky, 2002; Fox, 2003; Chaufray *et al.*, 2007].

[16] At the time of this writing, the MCD did not include any volume mixing ratios for Ar, O₂, NO, or He, listed here in order of decreasing abundance at 140 km as measured by the Viking Landers [Nier and McElroy, 1977]. Ar has been added with a volume mixing ratio of 60% that of N₂ at 80 km [F. Forget, 2011, personal communication] and

Table 1. A Brief Survey of Measured Exospheric Atomic Hydrogen at Mars Between 200 and 400 km

ρ_{exo} (cm ⁻³)	T_{∞} ^a (K)	Solar activity	Spacecraft	Source
2 × 10 ⁵	200 ^C	solar minimum	Rosetta	Feldman <i>et al.</i> [2011]
9 × 10 ⁴	260 ^H	solar minimum	Rosetta	Feldman <i>et al.</i> [2011]
10 ⁴	>600 ^H	solar minimum	ASPERA-3/NDP	Galli <i>et al.</i> [2006]
1–4 × 10 ⁵	200–250	solar minimum	SPICAM	Chaufray <i>et al.</i> [2008]
3 × 10 ⁴	350 ^H	solar maximum	Mariners 6, 7	Anderson and Hord [1971]
2.5 × 10 ⁴	350 ^H	solar maximum	Mariners 6, 7	Anderson and Hord [1972]
6 × 10 ³	350 ^H	solar maximum	Mars-3	Dementyeva <i>et al.</i> [1972]

ρ_{exo} is exospheric density which varies little in that altitude range. T_{∞} is exospheric temperature.

^aC refers to the cold (photochemically generated) component of atomic hydrogen and H to the hot component (due to charge exchange with the solar wind). In this model, the cold population densities are adopted. Interested readers are referred to Lichtenegger *et al.* [2004, 2006] for a more complete discussion of the separate populations.

agrees with Ar density profiles measured by Viking. O₂, NO, and He neutral species have been neglected in the current model. Ignoring these neutral species has negligible effects (<1%) on the density propagation of the included neutrals. Omitting these species from the model chemistry has similarly negligible effects on the production of major ions (discussed in more detail below).

[17] The resulting neutral atmosphere, adopted from the MCD and adjusted to the constraints set by Mendillo *et al.* [2011] for the conditions used for MGS, with the addition of atomic H and Ar, is shown in Figure 1. The solid lines show

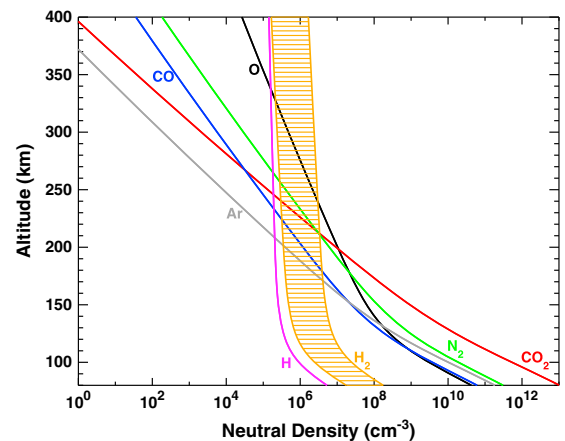


Figure 1. Neutral atmosphere used. The profiles include the standard five MCD neutral species (CO₂, O, N₂, CO, and H₂) used in Mendillo *et al.* [2011] for the MGS case. H has been added and is constrained to agree with remote sensing measurements at solar minimum. Argon has also been included by choosing 60% of the volume mixing ratio of N₂ at 80 km to this species (see Section 2.1 for details). The shaded region indicates the range of H₂ densities used for this study. The upper and lower limits correspond to the MCD and Krasnopolsky [2002] modeled values, respectively.

the density profiles as generated for all species under consideration. The shaded region shows the uncertainty in H_2 estimated densities, the limits of which will be used in the first of two sensitivity experiments described in Sections 3.1.1 and 3.2.1. The lower limit of H_2 (dashed line) conforms to values modeled for solar minimum conditions and that are based on FUSE observations of H_2 at high solar activity. The upper limit of H_2 (solid line) is derived from the MCD.

2.2. Updates to Ion Chemistry

[18] Photons either directly or dissociatively ionize neutrals. Photo-ionization of CO into O^+ and of CO_2 into O^+ and CO^+ have been added to the model. The addition of H and H_2 neutrals to the model of *Mendillo et al.* [2011] results in their ionization and subsequent inclusion in additional chemistry. As a result, the following seven primary ions are obtained: CO_2^+ , N_2^+ , O^+ , CO^+ , Ar^+ , H_2^+ , and H^+ . These ions then react with neutrals to give the secondary ions: O_2^+ , NO^+ , H_3^+ , OH^+ , HCO^+ , ArH^+ , N_2H^+ , HCO_2^+ , and HOC^+ . While the isomers HOC^+ and HCO^+ have similar reactions and reaction rates, they are separate species and are treated as such [*Rosati et al.*, 2007]. A complete list of reactions considered in the model used for the present work is shown in Table 2. Each of the 16 ions is tracked individually through altitude and local time, and the ion concentrations are summed to obtain an electron density.

[19] The reaction rate, k_1 (see Table 2), between H^+ and H_2 resulting in the production of H_2^+ is unconstrained at Mars and is the second (and final) sensitivity test to the model described in this paper as discussed in Sections 3.1.2 and 3.2.2. The charge exchange reaction rate between H^+ and H_2 is estimated to be $10^{-9} \text{ cm}^3 \text{ s}^{-1}$ [*Cravens*, 1987]. This reaction is exothermic for hydrogen molecules that are in the vibrational states (v) greater than 4. The reaction rate, k_1 , is then a function of the abundance of this state of H_2 ($v \geq 4$). This reaction has been studied for Saturn, and the rate coefficient adopted from *Cravens* [1987] is considered an upper limit [*Huestis et al.*, 2008]. As a result, k_1 has been adjusted to be $\sim 10^{-14} \text{ cm}^3 \text{ s}^{-1}$ for Saturn simulations [*Moses and Bass*, 2000; *Moore et al.*, 2004]. An overview of the hydrogen chemistry relevant to outer planets can be found in *Hallett et al.* [2005] and *Nagy et al.* [2009]. It is not clear if this reaction is as crucial on Mars as it is on the gas giants with their predominantly hydrogen atmospheres. The impact of this reaction on the composition of the ionosphere is tested, for the first time for Mars, by using the extreme values of 0 and $10^{-9} \text{ cm}^3 \text{ s}^{-1}$ to study its effects on modeled ion densities.

[20] Reactions that involve a combination of minor neutrals, minor ions, and slower reaction rates ($\leq 10^{-11} \text{ cm}^3 \text{ s}^{-1}$) that were not already used in the reference model have been neglected. Furthermore, the chemistry involving O_2 , NO, He, and their photo ions have been neglected since the parent neutral densities are minor and the volume mixing ratios are not constrained by the MCD at the time of this work. The photochemical ions suppressed due to the exclusion of these neutrals are N^+ , NH^+ , HeH^+ , C^+ , NH_2^+ , NCO^+ , HNO^+ , NH_3^+ , and NH_4^+ . The untreated photochemistry also leads to an underproduction of modeled NO^+ and HCO^+ and to an overproduction of modeled H^+ , H_2^+ , OH^+ , O_2^+ , and Ar^+ . While the cumulative effects of ignoring O_2 ,

He, and NO chemistry on the under/over production of ions do not affect the conclusions of this work, we recognize that some of the chemical pathways excluded from the model may eventually be found to be significant.

2.3. Updates to Diffusion Physics

[21] With the addition of several ion species, collisions among ions become comparable to collisions between ions and neutrals at altitudes where ion diffusion dominates plasma motion ($>150 \text{ km}$). Ion-ion collisions were added to the momentum equation calculations of vertical ion velocity in the model used for this work [*Banks and Kockarts*, 1973].

[22] Dealing with the complex geometry of plasma diffusion affected by crustal or draped magnetic field configurations is not a task suited to a 1-D model. In this work, we explore effects of chemistry in a photochemical-only scenario, and in a photochemical plus vertical transport scenario. The resulting ion and electron concentrations describe the topside ionosphere composition that would then be subjected to horizontal, transport, and/or solar wind pick-up effects.

3. Results

[23] The focus of this work is to analyze the topside composition of the Martian ionosphere. Introducing H and H_2 chemistry into the model has led to the generation of the new hydrogenated ions: H^+ , H_2^+ , H_3^+ , OH^+ , HCO^+ , ArH^+ , N_2H^+ , HCO_2^+ , and HOC^+ as well as CO^+ and Ar^+ . The ionospheric composition above 200 km clearly varies based on the various simulation conditions used. For the work presented here, all model input is fixed except for two sensitivity parameters that are examined for effects on the upper ionosphere. These two parameters are (1) the H_2 mixing ratio at 80 km and (2) the $H^+ + H_2$ charge exchange reaction rate, k_1 . The sensitivity tests are run for the case of (a) photochemistry only and (b) photochemistry plus vertical transport, as described next.

3.1. Effects on Photochemistry

[24] Beginning with the case of photochemistry only (no vertical transport), the sensitivity of the ionosphere to H_2 mixing ratio is tested while k_1 is held constant. Next, the sensitivity to the reaction rate, k_1 , is tested while holding the H_2 mixing ratio constant.

3.1.1. Sensitivity to H_2

[25] The sensitivity of the ionospheric composition to H_2 mixing ratio at 80 km is tested by setting the lower limit to 1.6 ppm, and the upper limit to 16 ppm. The former scenario is referred to as case A, and the latter as case B. For this analysis, k_1 is kept fixed at its lower limit of 0, effectively suppressing reaction 1 in Table 2. The difference between using the lower and upper limits of H_2 affects the photoproduction of both H^+ and H_2^+ and also the consequent chemistry.

[26] Figure 2 shows the resulting noontime density profiles for this simulation. In Figure 2a, electron densities show the effects of varying the H_2 neutral density from lower to upper limits given by the dashed to solid lines, respectively. The overall electron density shows insensitivity to H_2 except in the topside ionosphere where it increases with increasing H_2 . Figure 2b shows the ion density profile ranges with shaded regions of ion densities, bounded by the dashed and solid lines that correspond to low and high limits of

Table 2. A Complete List of Ionization (I), Chemical, and Recombination (R) Reactions Considered for This Work

		Ionization reaction	
11		$H + hv \rightarrow H^+ + e^-$	
12		$H_2 + hv \rightarrow H_2^+ + e^-$	
13		$H_2 + hv \rightarrow H^+ + H + e^-$	
14		$O + hv \rightarrow O^+ + e^-$	
15		$N_2 + hv \rightarrow N_2^+ + e^-$	
16		$CO + hv \rightarrow CO^+ + e^-$	
17		$CO + hv \rightarrow O^+ + C + e^-$	
18		$Ar + hv \rightarrow Ar^+ + e^-$	
19		$CO_2 + hv \rightarrow CO_2^+ + e^-$	
110		$CO_2 + hv \rightarrow O^+ + CO + e^-$	
111		$CO_2 + hv \rightarrow CO^+ + O + e^-$	
	Reaction	Reaction rate ^a ($cm^3 s^{-1}$)	Reference
1	$H^+ + H_2 \rightarrow H_2^+ + H$	$k_1 = 1 \times 10^{-9b}$	Cravens [1987]
2	$H^+ + O \rightarrow O^+ + H$	$k_2 = 3.75 \times 10^{-10}$	Anicich and Huntress [1986]
3	$H^+ + CO_2 \rightarrow HCO^+ + O$	$k_3 = 3.8 \times 10^{-9}$	Moses and Bass [2000]
4	$H_2^+ + H \rightarrow H^+ + H_2$	$k_4 = 6.4 \times 10^{-10}$	Anicich and Huntress [1986]
5	$H_2^+ + H_2 \rightarrow H_3^+ + H$	$k_5 = 2.0 \times 10^{-9}$	Kim and Fox [1994]
6	$H_2^+ + O \rightarrow OH^+ + H$	$k_6 = 1.5 \times 10^{-9}$	Krasnopolsky [2002]
7	$H_2^+ + N_2 \rightarrow N_2H^+ + H$	$k_7 = 2.0 \times 10^{-9}$	Anicich and Huntress [1986]
8	$H_2^+ + CO \rightarrow HCO^+ + H$	$k_8 = 2.16 \times 10^{-9}$	Anicich and Huntress [1986]
9	$H_2^+ + CO \rightarrow CO^+ + H_2$	$k_9 = 6.44 \times 10^{-10}$	Anicich and Huntress [1986]
10	$H_2^+ + Ar \rightarrow ArH^+ + H$	$k_{10} = 1.24 \times 10^{-9}$	Anicich [1993]
11	$H_2^+ + CO_2 \rightarrow HCO_2^+ + H$	$k_{11} = 2.35 \times 10^{-9}$	Anicich and Huntress [1986]
12	$H_3^+ + O \rightarrow OH^+ + H_2$	$k_{12} = 8.0 \times 10^{-10}$	Anicich and Huntress [1986]
13	$H_3^+ + N_2 \rightarrow N_2H^+ + H_2$	$k_{13} = 1.3 \times 10^{-9}$	Anicich [1993]
14	$H_3^+ + CO \rightarrow HCO^+ + H_2$	$k_{14} = 1.7 \times 10^{-9}$	Anicich [1993]
15	$H_3^+ + Ar \rightarrow ArH^+ + H_2$	$k_{15} = 3.65 \times 10^{-10}$	Anicich and Huntress [1986]
16	$H_3^+ + CO_2 \rightarrow HCO_2^+ + H_2$	$k_{16} = 2.0 \times 10^{-9}$	Anicich and Huntress [1986]
17	$O^+ + H \rightarrow H^+ + O$	$k_{17} = 6.4 \times 10^{-10}$	Moses and Bass [2000]
18	$O^+ + H_2 \rightarrow OH^+ + H$	$k_{18} = 1.67 \times 10^{-9}$	Anicich [1993]
19	$O^+ + N_2 \rightarrow NO^+ + N$	$k_{19} = 1.2 \times 10^{-12}$	Schunk and Nagy [2009]
20	$O^+ + CO_2 \rightarrow O_2^+ + CO$	$k_{20} = 1.1 \times 10^{-9}$	Schunk and Nagy [2009]
21	$OH^+ + O \rightarrow O_2^+ + H$	$k_{21} = 7.1 \times 10^{-10}$	Millar et al. [1997]
22	$OH^+ + N_2 \rightarrow N_2H^+ + O$	$k_{22} = 2.4 \times 10^{-10}$	Anicich [1993]
23	$OH^+ + CO \rightarrow HCO^+ + O$	$k_{23} = 3.55 \times 10^{-10}$	Anicich [1993]
24	$OH^+ + CO \rightarrow CO^+ + OH$	$k_{24} = 3.55 \times 10^{-10}$	Anicich [1993]
25	$OH^+ + CO_2 \rightarrow HCO_2^+ + O$	$k_{25} = 1.1 \times 10^{-9}$	Anicich [1993]
26	$N_2^+ + H_2 \rightarrow N_2H^+ + H$	$k_{26} = 2.0 \times 10^{-9}$	Anicich [1993]
27	$N_2^+ + O \rightarrow O^+ + N_2$	$k_{27} = 9.8 \times 10^{-12}$	Schunk and Nagy [2009]
28	$N_2^+ + O \rightarrow NO^+ + N$	$k_{28} = 1.3 \times 10^{-10}$	Schunk and Nagy [2009]
29	$N_2^+ + CO_2 \rightarrow CO_2^+ + N_2$	$k_{29} = 8.0 \times 10^{-10}$	Schunk and Nagy [2009]
30	$CO^+ + H_2 \rightarrow HCO^+ + H$	$k_{30} = 7.5 \times 10^{-10}$	Scott et al. [1997]
31	$CO^+ + H_2 \rightarrow HOC^+ + H$	$k_{31} = 7.5 \times 10^{-10}$	Scott et al. [1997]
32	$CO^+ + H \rightarrow H^+ + CO$	$k_{32} = 4.0 \times 10^{-10}$	Scott et al. [1997]
33	$CO^+ + O \rightarrow O^+ + CO$	$k_{33} = 1.4 \times 10^{-10}$	Anicich and Huntress [1986]
34	$CO^+ + CO_2 \rightarrow CO_2^+ + CO$	$k_{34} = 1 \times 10^{-9}$	Anicich and Huntress [1986]
35	$N_2H^+ + CO_2 \rightarrow HCO_2^+ + N_2$	$k_{35} = 1.4 \times 10^{-9}$	Anicich and Huntress [1986]
36	$N_2H^+ + O \rightarrow OH^+ + N_2$	$k_{36} = 1.4 \times 10^{-10}$	Anicich and Huntress [1986]
37	$N_2H^+ + CO \rightarrow HCO^+ + N_2$	$k_{37} = 8.8 \times 10^{-10}$	Anicich and Huntress [1986]
38	$HOC^+ + H_2 \rightarrow H_3^+ + CO$	$k_{38} = 2.35 \times 10^{-10}$	Anicich [1993]
39	$HOC^+ + H_2 \rightarrow HCO^+ + H_2$	$k_{39} = 2.35 \times 10^{-10}$	Anicich [1993]
40	$HOC^+ + CO \rightarrow HCO^+ + CO$	$k_{40} = 6 \times 10^{-10}$	Anicich [1993]
41	$HOC^+ + CO_2 \rightarrow HCO_2^+ + CO$	$k_{41} = 9 \times 10^{-10}$	Anicich [1993]
42	$Ar^+ + H_2 \rightarrow ArH^+ + H$	$k_{42} = 7.7 \times 10^{-10}$	Anicich [1993]
43	$Ar^+ + CO_2 \rightarrow CO_2^+ + Ar$	$k_{43} = 4.4 \times 10^{-10}$	Anicich [1993]
44	$ArH^+ + H_2 \rightarrow H_3^+ + Ar$	$k_{44} = 9 \times 10^{-10}$	Anicich [1993]
45	$ArH^+ + CO \rightarrow HCO^+ + Ar$	$k_{45} = 1.25 \times 10^{-9}$	Anicich [1993]
46	$ArH^+ + CO_2 \rightarrow HCO_2^+ + Ar$	$k_{46} = 1 \times 10^{-9}$	Anicich [1993]
47	$CO_2^+ + H \rightarrow H^+ + CO_2$	$k_{47} = 5.53 \times 10^{-11}$	Moses and Bass [2000]
48	$CO_2^+ + H \rightarrow HCO^+ + O$	$k_{48} = 4.7 \times 10^{-10}$	Krasnopolsky [2002]
49	$CO_2^+ + H_2 \rightarrow HCO_2^+ + H$	$k_{49} = 8.7 \times 10^{-10}$	Scott et al. [1997]
50	$CO_2^+ + O \rightarrow O^+ + CO_2$	$k_{50} = 9.6 \times 10^{-11}$	Schunk and Nagy [2009]
51	$CO_2^+ + O \rightarrow O_2^+ + CO$	$k_{51} = 1.6 \times 10^{-10}$	Schunk and Nagy [2009]
52	$HCO_2^+ + N_2 \rightarrow N_2H^+ + CO_2$	$k_{52} = 1.37 \times 10^{-9}$	Anicich and Huntress [1986]
	Reaction	Recombination rate ^c ($cm^3 s^{-1}$)	Reference
R1	$H^+ + e^- \rightarrow H$	$\alpha_1 = 4.22 \times 10^{-12} \times (300/T_e)^{0.7}$	Schunk and Nagy [2009]
R2	$H_2^+ + e^- \rightarrow H + H$	$\alpha_2 = 2.3 \times 10^{-7} \times (300/T_e)^{0.4}$	Kim and Fox [1994]
R3	$H_3^+ + e^- \rightarrow H + H_2$	$\alpha_3 = 4.4 \times 10^{-8} \times (300/T_e)^{0.5}$	Kim and Fox [1994]
R4	$H_3^+ + e^- \rightarrow H + H + H$	$\alpha_4 = 5.6 \times 10^{-8} \times (300/T_e)^{0.5}$	Kim and Fox [1994]
R5	$O^+ + e^- \rightarrow O$	$\alpha_5 = 3.26 \times 10^{-12} \times (300/T_e)^{0.7}$	Schunk and Nagy [2009]
R6	$OH^+ + e^- \rightarrow O + H$	$\alpha_6 = 3.75 \times 10^{-8} \times (300/T_e)^{0.5}$	Moses and Bass [2000]
R7	$N_2^+ + e^- \rightarrow N + N$	$\alpha_7 = 2.2 \times 10^{-7} \times (300/T_e)^{0.39}$	Schunk and Nagy [2009]

Table 2. (continued)

		Ionization reaction	
R8	$\text{CO}^+ + e^- \rightarrow \text{O} + \text{C}$	$\alpha_8 = 2.75 \times 10^{-7} \times (300/T_e)^{0.5}$	<i>Schunk and Nagy</i> [2009]
R9	$\text{N}_2\text{H}^+ + e^- \rightarrow \text{N} + \text{N} + \text{H}$	$\alpha_9 = 8.66 \times 10^{-7} \times (300/T_e)^{0.5}$	<i>Mul and McGowan</i> [1979]
R10	$\text{HCO}^+ + e^- \rightarrow \text{CO} + \text{H}$	$\alpha_{10} = 1.1 \times 10^{-7} \times (300/T_e)$	<i>Moses and Bass</i> [2000]
R11	$\text{HOC}^+ + e^- \rightarrow \text{CO} + \text{H}$	$\alpha_{11} = 1.1 \times 10^{-7} \times (300/T_e)$	<i>Liszt et al.</i> [2004]
R12	$\text{NO}^+ + e^- \rightarrow \text{N} + \text{O}$	$\alpha_{12} = 4.0 \times 10^{-7} \times (300/T_e)^{0.5}$	<i>Schunk and Nagy</i> [2009]
R13	$\text{O}_2^+ + e^- \rightarrow \text{O} + \text{O}$	$\alpha_{13} = 2.4 \times 10^{-7} \times (300/T_e)^{0.7}$	<i>Schunk and Nagy</i> [2009]
R14	$\text{Ar}^+ + e^- \rightarrow \text{Ar}$	$\alpha_{14} = 10^{-10}$	<i>Gu</i> [2003]
R15	$\text{ArH}^+ + e^- \rightarrow \text{Ar} + \text{H}$	$\alpha_{15} = 10^{-9}$	<i>Mitchell et al.</i> [2005]
R16	$\text{CO}_2^+ + e^- \rightarrow \text{CO} + \text{O}$	$\alpha_{16} = 4.2 \times 10^{-7} \times (300/T_e)^{0.75}$	<i>Schunk and Nagy</i> [2009]
R17	$\text{HCO}_2^+ + e^- \rightarrow \text{OH} + \text{CO}$	$\alpha_{17} = 1.1 \times 10^{-7} \times (300/T_e)^{0.5}$	<i>Herd et al.</i> [1990]
R18	$\text{HCO}_2^+ + e^- \rightarrow \text{CO}_2 + \text{H}$	$\alpha_{18} = 3.4 \times 10^{-7} \times (300/T_e)^{0.5}$	<i>Krasnopolsky</i> [2000]

T_e is the electron temperature in Kelvin.

^aWhen applicable, branching ratios are included in the reaction rate.

^b k_1 represents an estimate of the reaction rate (see text).

^cWhen applicable, branching ratios are included in the recombination rate.

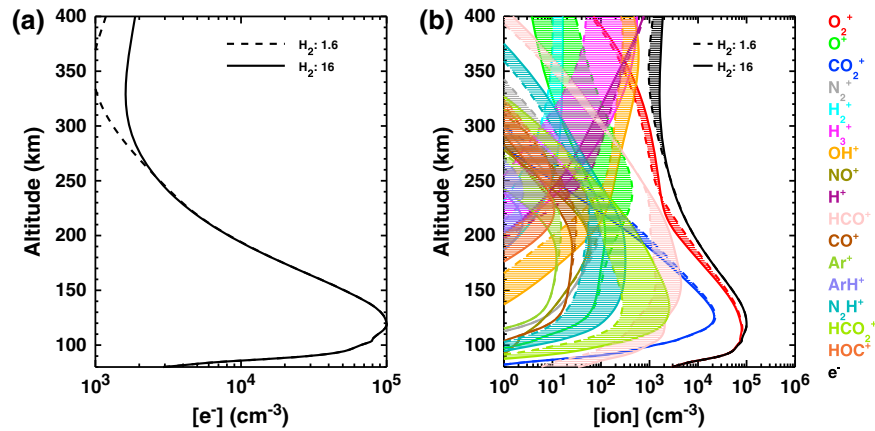


Figure 2. Modeled electron and ion densities vs. altitude for midday conditions. The reaction rate k_1 is $0 \text{ cm}^3 \text{ s}^{-1}$; the model is set for photochemistry only. (a) The electron density profiles resulting from varying the H_2 mixing ratio from low to high values of 1.6 to 16 ppm at 80 km are shown in dashed and solid black, respectively. (b) The ion densities range between using low and high mixing ratios of H_2 .

H_2 densities (cases A and B, respectively). As the H_2 mixing ratio increases, the production rates of H_3^+ , OH^+ , N_2H^+ , HCO^+ , and HCO_2^+ increase, and the loss rates of H^+ , O^+ , N_2^+ , CO^+ , Ar^+ , and CO_2^+ increase. The ion abundances of H_2^+ , O_2^+ , NO^+ , HOC^+ , and ArH^+ are affected by both increased production and loss resulting in net effects of increased H_2^+ , decreased HOC^+ , unchanging NO^+ , and varying increases and decreases in O_2^+ and ArH^+ with altitude. In response to the increase in H_2 , the decreases in CO_2^+ and O^+ cause O_2^+ abundances to decrease below 220 km. The increase in OH^+ causes the O_2^+ abundance to increase above that altitude. The ion concentration at each altitude is determined by the choice of H_2 mixing ratio.

[27] In this and remaining subsections, the ion composition is listed in percent ranging from the simulation where the lower limit of a sensitivity parameter was used to the simulation where the upper limit of a sensitivity parameter was used. The first percentage summarizes case A and the second case B at 350 km. For the photochemical-only simulations where $k_1 = 0 \text{ cm}^3 \text{ s}^{-1}$ and the H_2 mixing ratio varies between 1.6 and 16 ppm at 80 km, the resulting ionospheric composition at 350 km in order of decreasing abundance is OH^+ (27–36%), O_2^+

(30–25%), H^+ (30–11%), H_3^+ (2–24%), O^+ (7–0.5%), H_2^+ (~1%), HCO^+ (~1%), N_2H^+ , and others are each <1%.

3.1.2. Sensitivity to k_1

[28] The second sensitivity test studies the effects of reaction 1 in Table 2. For photochemical-only simulations, the sensitivity test for k_1 is conducted by fixing the H_2 mixing ratio at the middle value of 9 ppm at 80 km and by varying k_1 from a lower limit value of 0 to an upper limit value of $10^{-9} \text{ cm}^3 \text{ s}^{-1}$ (referred to as cases C and D, respectively). Figure 3 shows the results of this test for noontime conditions. Figure 3a shows the effects of varying k_1 on the electron density from lower to upper limits given by dashed to solid lines, respectively. Only the high-altitude electron density is affected by k_1 , showing a small decrease with increasing reaction rate. Figure 3b shows the ion density profile ranges of ion densities, using the same format as in Figure 2. It is clear that the shading that spans the dashed and solid lines is appreciable only for a single ion (H^+). As k_1 increases, the production rate of H_2^+ increases (from the loss of H^+), resulting in an increase of H_3^+ , HCO^+ , and N_2H^+ production. Loss of H^+ also causes a decrease in the O^+ production. Densities of ions at lower altitudes are unaffected by

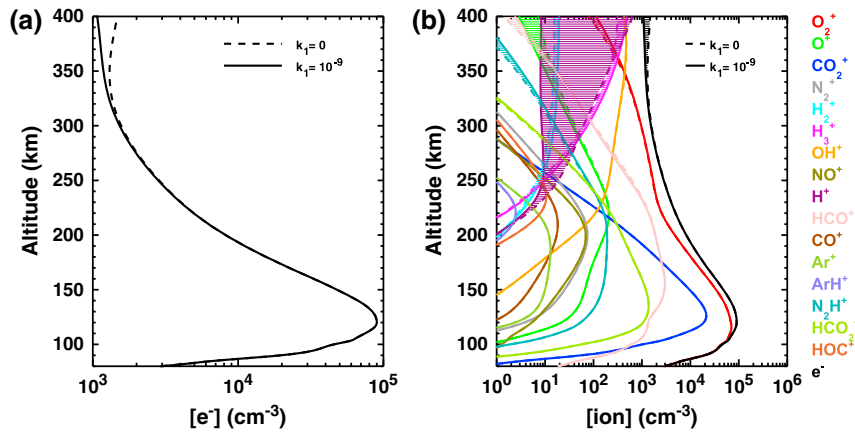


Figure 3. Same format as Figure 2. The mixing ratio for H_2 is set to a middle value of 9 ppm at 80 km and the model is set for photochemistry only. (a) The electron densities resulting from varying the k_1 reaction rate from low to high values of 0 and $10^{-9} \text{ cm}^3 \text{ s}^{-1}$ are shown in dashed and solid black, respectively. (b) The ion densities range between using low and high reaction rate values of k_1 .

the changing reaction rate due to the absence of significant concentrations of H^+ and H_2^+ below 200 km.

[29] For this simulation, with an H_2 mixing ratio of 9 ppm at 80 km and k_1 varying between 0 and $10^{-9} \text{ cm}^3 \text{ s}^{-1}$, the resulting ionospheric composition at 350 km in order of decreasing abundance is OH^+ (34–37%), O_2^+ (30–36%), H_3^+ (16–22%), H^+ (16–0.7%), H_2^+ (~1%), HCO^+ (~1%), and O^+ (~1%), N_2H^+ and others are each <1%. As in the previous subsection, the percentages range from the simulation where the lower limit of k_1 was used (case C) to the simulation where the upper limit of k_1 was used (case D).

3.2. Effects on Photochemistry with Vertical Transport

[30] Having assessed the effects that hydrogen chemistry can cause upon the plasma constituents throughout the ionosphere, the next set of simulations addresses the influence of coupled chemistry and plasma transport. Previous studies have shown that plasma diffusion becomes important in the topside ionosphere, and thus, a more comprehensive treatment of plasma dynamics is used.

3.2.1. Sensitivity to H_2

[31] A similar test is done as for the photochemical-only case by now allowing ions to diffuse vertically. Figure 4 shows the effects of varying H_2 while keeping k_1 fixed at 0, referred to as cases E and F. Figure 4a gives the electron density concentrations varying between the dashed and solid black lines as the H_2 volume mixing ratio is varied from lower to upper limits of 0 and 16 ppm, respectively. Figure 4b shows the ion density profile ranges with shaded regions of ion densities, bounded by the dashed and solid lines that correspond to these low and high limits of H_2 .

[32] For this simulation, $k_1 = 0 \text{ cm}^3 \text{ s}^{-1}$ and the H_2 mixing ratio varies between 1.6 and 16 ppm at 80 km. The resulting ionospheric composition at 350 km in order of decreasing abundance is HCO^+ (24–87%), O_2^+ (62–6%), O^+ (6–0.3%), OH^+ (2–4%), CO_2^+ (3–0.04%), and others are each <1%. The percentages range from the simulation where the lower limit of the H_2 mixing ratio was used (case E) to the simulation where the upper limit of the H_2 mixing ratio was used (case F).

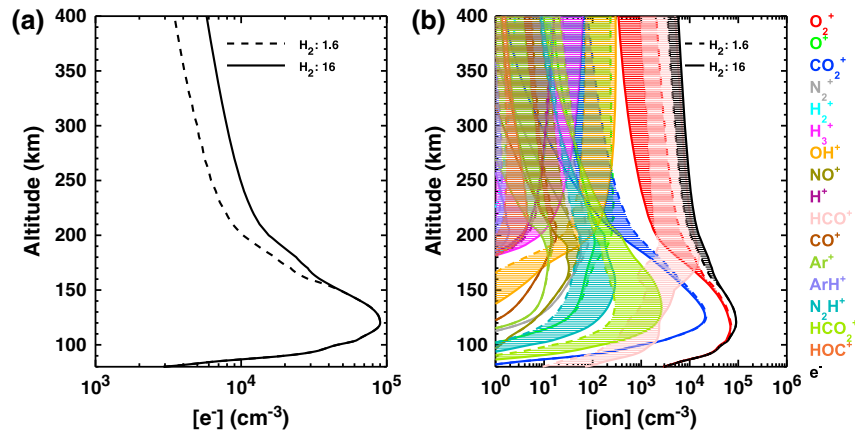


Figure 4. Same format as Figure 2. The reaction rate k_1 is 0, the model is set for chemistry plus vertical transport. (a) The electron density profiles resulting from varying the H_2 mixing ratio from low to high values of 1.6 to 16 ppm at 80 km are shown in dashed and solid black, respectively. (b) The ion densities range between using low and high mixing ratios of H_2 .

3.2.2. Sensitivity to k_1

[33] The case of keeping H_2 at a fixed volume mixing ratio of 9 ppm and varying k_1 from 0 to $10^{-9} \text{ cm}^3 \text{ s}^{-1}$ and including vertical transport is shown in Figure 5. These simulations are referred to as cases G and H, respectively. The ionospheric composition varies by few ions per cubic centimeter, and the overall electron density for each limiting case is the same as is shown in Figure 5a. The ionospheric composition variation is limited to HCO^+ , O_2^+ , and H^+ densities.

[34] For this simulation, the H_2 mixing ratio is 9 ppm at 80 km, and k_1 varies between 0 and $10^{-9} \text{ cm}^3 \text{ s}^{-1}$. The resulting ionospheric composition at 350 km in order of decreasing abundance is shown in Figure 5b as O_2^+ (57%), HCO^+ (30%), OH^+ (4%), O^+ (2%), HCO_2^+ (2%), N_2H^+ (1%), and CO_2^+ (1%), and others are each $<1\%$. The percentages range from the simulation where the lower limit of k_1 was used (case G) to the simulation where the upper limit of k_1 was used (case H). Variability in the major ionospheric composition due to lower and upper limits of k_1 in this case is negligible.

3.3. Effects of Ion-Ion Collisions

[35] Models of planetary ionospheres often incorporate ion-ion collisions into the equations of motion (e.g., *Chen and Nagy* [1978] for Venus; *Millward et al.* [1996] for Earth; *Moore et al.* [2004] for Saturn). The model used here was adapted from *Mendillo et al.* [2011] that incorporated ion-neutral collisions only. Including ion-ion interactions into the model slows down ion diffusion and leads to larger ion and electron densities when compared with the case of ion-neutral interactions only. The overall increase in electron density at 400 km is 15–75%, varying with choice of H_2 mixing ratio at 80 km and k_1 reaction rate used. In Figure 6, the effects of including ion-ion collisions in the ionosphere of Mars is demonstrated for the case of H_2 mixing ratio of 16 ppm at 80 km and k_1 of $0 \text{ cm}^3 \text{ s}^{-1}$ (case F).

3.4. Summary of Sensitivity Tests

[36] The ionospheric composition sensitivity to the scenarios discussed and plotted in this section is summarized in

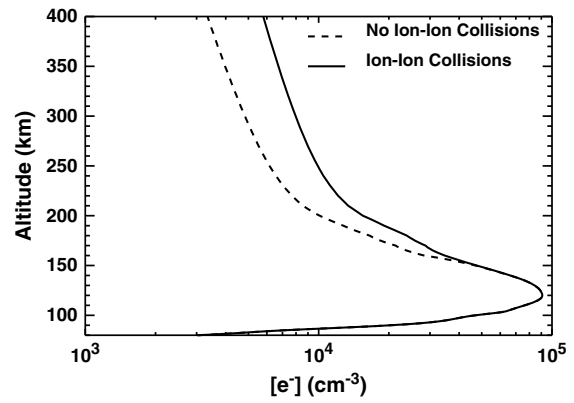


Figure 6. Effects of including ion-ion collisions on electron density. The H_2 mixing ratio at 80 km is 16 ppm, the k_1 reaction rate is 0, and the model is set for chemistry plus vertical transport. The electron density profiles are shown for noontime conditions with the dashed line representing the case of ion-neutral collisions only and the solid line representing the addition of ion-ion collisions.

Table 3. When k_1 is fixed and the amount of atmospheric H_2 increases, photo-ionization of H_2 into H^+ and H_2^+ increases and, consequently, the electron density increases. This trend is shown in the electron density profiles shown in Figures 2a and 4a. When the H_2 density is fixed and k_1 increases, the reaction between H^+ and H_2 provides a loss mechanism that prevents the buildup of H^+ , thereby decreasing the overall H^+ density, causing the electron density to decrease, as is shown in Figure 3a but is imperceptible in Figure 5a. For the case of photochemistry only, the electron density increases by about 55% and decreases by 10% at 350 km when H_2 or k_1 are increased, respectively. For the case of vertical transport, the electron density increases by $\sim 65\%$ as a response to increasing the H_2 mixing ratio and is negligibly affected by any changes in the reaction rate, k_1 . The effects of H_2 neutral density uncertainty on the ionospheric composition of Mars span all altitudes and impact the corresponding uncertainties of all the model ion densities

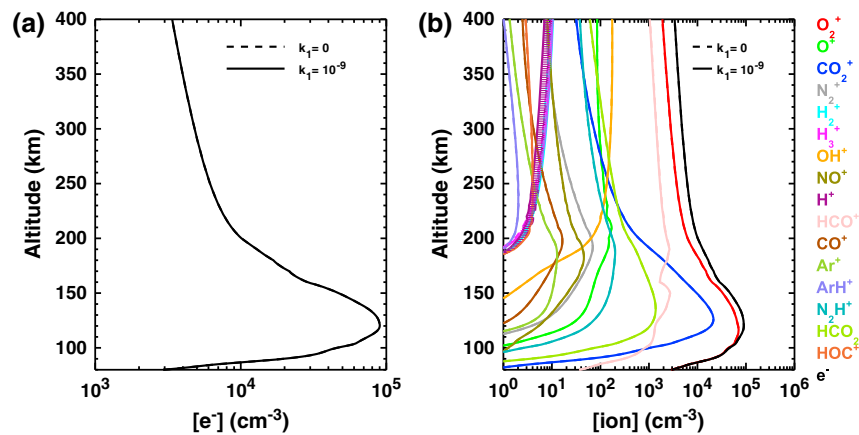


Figure 5. Same format as Figure 2. The mixing ratio for H_2 is set to a high value of 16 ppm at 80 km and the model is set for chemistry plus vertical transport. (a) The electron density profiles resulting from varying the k_1 reaction rate from a low to high value of 0 and $10^{-9} \text{ cm}^3 \text{ s}^{-1}$ are shown in dashed and solid black, respectively. The electron density profiles overlap as they are identical in both cases. (b) The ion densities range between using low and high reaction rate values of k_1 .

Table 3. A Summary of Sensitivity Parameters Considered in This Work^a

Case	Transport	H ₂ (ppm)	k ₁ (cm ³ s ⁻¹)	Abundances at 250 km	Abundances at 300 km	Abundances at 350 km	Section	[e ⁻] Plot	[Ion] Plot
A	None	1.6	0	O ₂ ⁺ (46%), HCO ⁺ (23%), O ⁺ (17%), OH ⁺ (5%), H ⁺ (2%), N ₂ ⁺ (2%), N ₂ H ⁺ (1%), CO ₂ ⁺ (1%), HCO ₂ ⁺ (1%), O ₂ ⁺ (59%), HCO ⁺ (22%), OH ⁺ (8%), N ₂ H ⁺ (3%), HCO ₂ ⁺ (3%), O ⁺ (2%)	O ₂ ⁺ (52%), OH ⁺ (16%), O ⁺ (14%), H ⁺ (10%), HCO ⁺ (6%)	O ₂ ⁺ (30%), H ⁺ (30%), OH ⁺ (27%), O ⁺ (7%), H ₃ ⁺ (2%), H ₂ ⁺ (1%)	3.1.1	2a, dashed	2b, dashed
B	None	16	0	O ₂ ⁺ (58%), HCO ⁺ (22%), OH ⁺ (7%), O ⁺ (5%), N ₂ H ⁺ (3%), HCO ₂ ⁺ (2%)	O ₂ ⁺ (58%), OH ⁺ (21%), H ₃ ⁺ (8%), HCO ⁺ (7%), H ⁺ (3%), O ⁺ (1%), N ₂ H ⁺ (1%)	OH ⁺ (36%), O ₂ ⁺ (25%), H ⁺ (11%), H ₃ ⁺ (24%), H ₂ ⁺ (1%), HCO ⁺ (1%)	3.1.1	2a, solid	2b, solid
C	None	9	0	O ₂ ⁺ (58%), HCO ⁺ (22%), OH ⁺ (7%), O ⁺ (5%), N ₂ H ⁺ (3%), HCO ₂ ⁺ (2%)	O ₂ ⁺ (61%), OH ⁺ (19%), HCO ⁺ (7%), H ⁺ (4%), H ₃ ⁺ (4%), O ⁺ (3%), N ₂ H ⁺ (1%)	OH ⁺ (34%), O ₂ ⁺ (30%), H ₃ ⁺ (16%), H ⁺ (16%), H ₂ ⁺ (1%), HCO ⁺ (1%)	3.1.2	3a, dashed	3b, dashed
D	None	9	10 ⁻⁹	O ₂ ⁺ (60%), HCO ⁺ (20%), OH ⁺ (7%), O ⁺ (5%), N ₂ H ⁺ (3%), HCO ₂ ⁺ (2%)	O ₂ ⁺ (63%), OH ⁺ (20%), HCO ⁺ (6%), H ₃ ⁺ (5%), O ⁺ (2%), N ₂ H ⁺ (1%), H ₂ ⁺ (1%)	OH ⁺ (37%), O ₂ ⁺ (36%), H ₃ ⁺ (22%), H ₂ ⁺ (1%), HCO ⁺ (1%), O ⁺ (1%)	3.1.2	3a, solid	3b, solid
E	Vertical	1.6	0	O ₂ ⁺ (67%), HCO ⁺ (21%), CO ₂ ⁺ (4%), O ⁺ (4%), HCO ₂ ⁺ (1%)	O ₂ ⁺ (54%), HCO ⁺ (35%), O ⁺ (4%), CO ₂ ⁺ (3%), OH ⁺ (1%)	HCO ⁺ (24%), O ₂ ⁺ (62%), O ⁺ (6%), OH ⁺ (2%), CO ₂ ⁺ (3%)	3.2.1	4a, dashed	4b, dashed
F	Vertical	16	0	HCO ⁺ (85%), O ₂ ⁺ (9%), OH ⁺ (2%), O ⁺ (1%)	HCO ⁺ (87%), O ₂ ⁺ (7%), OH ⁺ (4%)	HCO ⁺ (87%), O ₂ ⁺ (6%), OH ⁺ (4%)	3.2.1	4a, solid	4b, solid
G	Vertical	9	0	O ₂ ⁺ (60%), HCO ⁺ (28%), HCO ₂ ⁺ (3%), CO ₂ ⁺ (2%), OH ⁺ (2%), O ⁺ (2%), N ₂ H ⁺ (1%)	O ₂ ⁺ (59%), HCO ⁺ (30%), OH ⁺ (3%), O ⁺ (2%), HCO ₂ ⁺ (2%), N ₂ H ⁺ (1%), CO ₂ ⁺ (1%)	O ₂ ⁺ (57%), HCO ⁺ (30%), OH ⁺ (4%), O ⁺ (2%), HCO ₂ ⁺ (2%), N ₂ H ⁺ (1%), CO ₂ ⁺ (1%)	3.2.2	5a, dashed	5b, dashed
H	Vertical	9	10 ⁻⁹	Same as case G	Same as case G	Same as case G	3.2.2	5a, solid	5b, solid

^aH₂ is the mixing ratio by volume at 80 km. Abundances of ions greater than 1% at 250, 300, and 350 km are shown here. Details of each case are given in the text in the respective subsection listed.

and abundances. The uncertainty of the reaction rate, k_1 , for the same case of photochemistry only affects mainly the H⁺ density and has minor effects on other ions limited to altitudes where H⁺ is produced (>200 km). Ion-ion collisions were included in all the simulations presented for these cases.

4. Discussion

[37] The modeled HCO⁺ concentrations form a significant fraction of the Martian ionosphere. HCO⁺ is the third most abundant species below ~180 km after O₂⁺ and CO₂⁺. Above 180 km, HCO⁺ is second to and sometimes more abundant than O₂⁺.

[38] It is worth noting that the Viking Lander RPA instrument required a priori assumptions of the species being measured in order to model the measured number densities of these species [Nier et al., 1972; Hanson et al., 1977]. Best fits were achieved with the assumptions that combinations of O₂⁺, CO₂⁺, and O⁺ were the dominant ions between 130 and 220 km. The RPA data do not exclude the presence of HCO⁺ (29 amu mass species potentially obscured by 32 amu O₂⁺) or OH⁺ (17 amu mass species potentially obscured by 16 amu O⁺). HCO⁺ was also predicted to be an abundant ion by Krasnopolsky [2002]. Although Fox [2003] studied the effects of hydrogen on the ionosphere, the chemical scheme used did not include HCO⁺.

[39] The abundance of radio occultation profiles retrieved from MGS and MEX has allowed a detailed validation of the electron density concentration as a function of altitude for the model described here [Martinis et al., 2003; Mendillo et al., 2011; Lollo et al., 2012]. However, there are only two Viking Lander measurements of ion concentration at Mars.

[40] The ionospheric densities resulting from the simulations done for this work have been validated with the ion density profiles measured by the Viking1 Lander in Figure 7. RPA measurements of O₂⁺, O⁺, and CO₂⁺ from Hanson et al. [1977] were used for comparison with model cases A, B, E and F described in Figures 2 and 4 that show ion density variability due to H₂. An additional ion density profile for the sum of O₂⁺ and HCO⁺ is also shown for comparison. This is to account for any RPA measurements that could have resulted from Martian HCO⁺ being recorded as O₂⁺. In Figure 7a, the ion densities modeled for a lower limit of H₂ mixing ratio agree well with measurements for altitudes between 130 and 270 km for O₂⁺ (and O₂⁺ added to HCO⁺), for altitudes between 130 and 220 km for CO₂⁺ and at all altitudes for O⁺. Below 130 km, our modeled ion concentrations fall off with a similar shape to those measured by the RPA. The differences between model results and measurements below the main peak are attributed to the differences between the neutral atmosphere adopted in our model and that measured by Viking. Plasma dynamics that are not included in this simulation are likely responsible for the underestimation of modeled CO₂⁺ and overestimation of modeled O₂⁺ (despite agreement with O⁺) when compared with Viking 1 ion measurements at top altitudes. In Figure 7b, the simulation that includes vertical plasma transport (from Figure 4) is validated against the measurements. The agreement between the model and RPA measurements improves for CO₂⁺ at all altitudes and for O₂⁺ at the top side, while the model O⁺ concentrations intermittently underestimate measurements by at most a factor of 2.

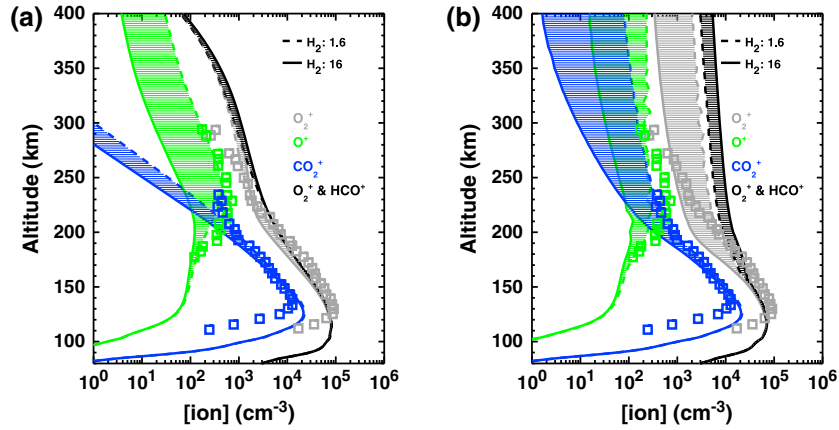


Figure 7. Model validation with Viking 1 ion measurements. RPA measurements of O_2^+ , O^+ , and CO_2^+ are shown in grey, green, and blue squares, respectively. The solid and dashed lines correspond to modeled densities using different H_2 abundances. The black lines correspond to combined O_2^+ and HCO^+ densities (see text in discussion section). (a) Comparison of the simulation shown in Figure 2b for $k_1 = 0 \text{ cm}^3 \text{ s}^{-1}$, H_2 ranging between 1.6 and 16 ppm by volume at 80 km and no transport. (b) Comparison of the simulation shown in Figure 4b for $k_1 = 0 \text{ cm}^3 \text{ s}^{-1}$, H_2 ranging between 1.6 and 16 ppm by volume at 80 km with vertical transport.

Table 4. A Comparison of Ion Densities Modeled in This Work for the Case Shown in Figure 2 With Other Modelers' Results at Similar Solar Cycle Conditions

Species and Altitude: Modeled Density Range (cm^{-3})	Density From Other Works (cm^{-3})	Source
O_2^+ at 200 km: $4\text{--}6 \times 10^3$	4×10^3	<i>Krasnopolsky</i> [2002]
CO_2^+ at 200 km: $4\text{--}8 \times 10^2$	1×10^3	<i>Krasnopolsky</i> [2002]
O^+ at 200 km: $1\text{--}2 \times 10^2$	1×10^2	<i>Krasnopolsky</i> [2002]
HCO^+ at 200 km: $1\text{--}2.5 \times 10^3$	6×10^2	<i>Krasnopolsky</i> [2002]
OH^+ at 200 km: $1\text{--}6 \times 10^1$	2×10^0	<i>Krasnopolsky</i> [2002]
N_2^+ at 200 km: $6\text{--}9 \times 10^1$	2×10^1	<i>Krasnopolsky</i> [2002]
NO^+ at 200 km: $5\text{--}9 \times 10^1$	2×10^1	<i>Krasnopolsky</i> [2002]
CO^+ at 200 km: $1\text{--}2 \times 10^1$	2×10^1	<i>Krasnopolsky</i> [2002]
Ar^+ at 200 km: $1\text{--}1.5 \times 10^1$	2×10^0	<i>Krasnopolsky</i> [2002]
N_2H^+ at 200 km: $0.5\text{--}3 \times 10^2$	8×10^{-1}	<i>Krasnopolsky</i> [2002]
HCO_2^+ at 200 km: $1\text{--}6 \times 10^2$	4×10^1	<i>Krasnopolsky</i> [2002]
H^+ at 220 km: $3\text{--}7 \times 10^0$	5×10^1	<i>Chen et al.</i> [1978]
	1×10^1	<i>Fox</i> [2003]
	8×10^{-1}	<i>Krasnopolsky</i> [2002]

[41] Due to the scarcity of measurements available at Mars of ion concentration with altitude, further comparison can only be done with other models. A summary of ion densities at a common altitude of 200–220 km is done in Table 4. The case shown in Figure 2 for photochemistry only with a lower limit of k_1 provides a good comparison to the model developed and discussed in *Krasnopolsky* [2002] for the solar minimum scenario. In his model, the charge exchange reaction k_1 is not considered (consistent with the lower limit in this work of $k_1 = 0$), H_2 has a mixing ratio at 80 km of 15 ppm (close to the upper limit in this work of 16 ppm), and at 300 km H_2 reaches a value that is close to the lower limit considered here. *Chen et al.* [1978] and *Fox* [2003] also provide models with some hydrogenated ions to compare the present results with.

[42] As summarized in Figure 7 and Table 4, the results of the model used for this work compare well with in situ measurements and some other models. Disagreement with remaining models is attributed to the different set of

photochemical reactions and reaction rates used in different simulations. For example, in this model, OH^+ is a major ion at upper altitudes. In a model by *Krasnopolsky* [2002], OH^+ is nearly an order of magnitude less abundant at similar altitudes for the same solar cycle conditions. A comparison of production and loss mechanisms between the model used here and that detailed in *Krasnopolsky* [2002] shows that the latter model does not include the production reaction between H_3^+ and O that produces much of the OH^+ at the topside ionosphere.

[43] Similar reasons explain the difference in HCO^+ densities between the two models. HCO^+ is produced as a secondary ion and can be generated through 10 channels listed in Table 2. The two main production mechanisms are due to CO_2^+ reacting with H and to N_2H^+ reacting with CO. Loss of HCO^+ occurs exclusively through recombination at a rate proportional to T_e^{-1} , much slower than the recombination rate of most other molecular ions. This leads to the gradual buildup of HCO^+ to large densities before reaching photochemical equilibrium. *Krasnopolsky's* model includes seven production reactions (four of which overlap with the model here) and a recombination rate similar to the one included in this work. Despite the differences in neutral and ion chemistry between *Krasnopolsky* [2002] and this work, both models project HCO^+ to be one of the most abundant ions below 200 km.

[44] The inclusion of H, H_2 , and associated hydrogenated ions in this model has resulted in the formation of an ionosphere that is no longer exclusively dominated by O_2^+ or O^+ at upper altitudes. For the photochemical-only case, the various sensitivity tests shown in this work yield an ionosphere that is dominated at 350 km by comparable densities of OH^+ , O_2^+ , H_3^+ , H^+ , and smaller quantities of O^+ , HCO^+ , H_2^+ , and N_2H^+ . In the case of full vertical plasma transport, O_2^+ and HCO^+ dominate at 350 km with smaller quantities of O^+ , OH^+ , and HCO_2^+ .

[45] Transport of ions becomes important above ~ 150 km. In transitioning from the photochemistry only to the

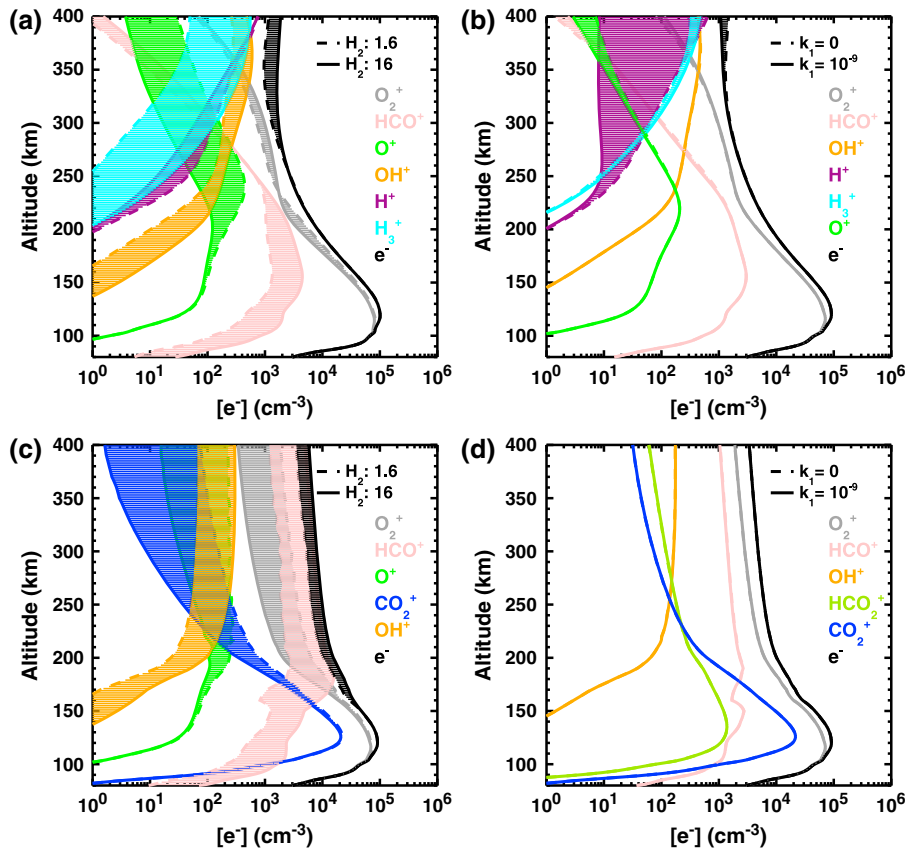


Figure 8. Overview of the most abundant species in the topside ionosphere for the eight cases simulated in this work. (a) As in Figure 2b, but neglecting ion species that are minor above 250 km. (b) As in Figure 3b, but neglecting ion species that are minor above 250 km. (c) As in Figure 4b, but neglecting ion species that are minor above 250 km. (d) As in Figure 5b, but neglecting ion species that are minor above 250 km. Color scheme has been changed slightly from that in Figures 2–5 for clarity.

photochemistry with vertical transport case, OH^+ , H_3^+ , and H^+ no longer dominate the ionosphere at 350 km because they have diffused downward, while both O_2^+ and HCO^+ have diffused upwards, resulting in the latter ions becoming a major ion species at top altitudes. The lighter ions diffuse downward and the heavier ions upward due to the dominating ion pressure term in the velocity calculations [Banks and Kockarts, 1973]. Due to chemistry, the ion density profiles of H^+ , H_2^+ , H_3^+ , and OH^+ increase with altitude as is shown in Figures 2b, 3b, 4b, and 5b. The resulting gradient in ion density with altitude (and consequently ion pressure) dictates the velocity direction, causing the lighter hydrogenated ions to diffuse to lower altitudes. The remaining ion abundances decrease with altitude, resulting in a negative density gradient and an upward velocity that dominates over the downward velocity from the gravity term, causing these ions to be transported to higher altitudes.

5. Conclusion

[46] A 1-D model of the Martian ionosphere [Mendillo et al., 2011], updated to include hydrogen chemistry and ion-ion collisions, shows that the composition of the topside ionosphere is very sensitive to the choice of neutral molecular hydrogen density, and less sensitive to the charge exchange reaction rate between H^+ and H_2 . Figure 8 and

Table 3 summarize the major ions that dominate the ionosphere above 250 km for the different simulations presented in this study.

[47] In the case of photochemistry only, the resulting dominant ions at 350 km are a combination of OH^+ , O_2^+ , H_3^+ , and H^+ and smaller quantities of O^+ , HCO^+ , H_2^+ , and N_2H^+ . For the case of vertical transport, the resulting dominant ions at 350 km are O_2^+ and HCO^+ with smaller quantities of O^+ , OH^+ , and HCO_2^+ . Ionospheric compositions at 250 and 300 km are further summarized in Table 3. Figures 2 through 5 show the detailed ionospheric composition for cases of the model that demonstrate sensitivity to uncertainties in H_2 neutral density and to the rate of a charge exchange reaction between H^+ and H_2 . The neutral density uncertainty has a larger impact on ionospheric composition than the reaction rate uncertainty. In all cases discussed in this paper, hydrogenated ions play a prominent role in the composition of the upper ionosphere of Mars.

[48] The results shown in this work are modeled for high-latitude locations at solar minimum noontime conditions. This model can be used in future work to investigate the diurnal and seasonal variability of the topside ionospheric composition, as well as to study the effects of solar cycle variability and varying magnetic field morphologies. A hint of the role of magnetic field (B) morphology possibly

emerges from these simulations. Yet, the accurate portrayal of such effects is beyond the capability of a 1-D model.

[49] The MAVEN mission will carry a set of instruments for studying atmospheric escape on Mars. The Neutral Gas and Ion Mass Spectrometer (NGIMS) instrument is capable of measuring and identifying the composition of thermal ions with masses ranging between 2 and 150 amu in situ at altitudes above 120 km. The resolution of the NGIMS is 1 amu, allowing measurements of HCO^+ (29 amu) to be distinguished from similar mass ions such as O_2^+ (32 amu) and N_2^+ (28 amu) [M. Benna, 2012, personal communication]. Its observations will test the predictions of this work and provide constraints for future modeling efforts.

[50] The ion densities generated in this work can offer an initial context for MAVEN NGIMS measurements between 150 and 400 km (depending on the height of the region separating ionospheric plasma from solar wind plasma at the time of measurement) and can therefore aid in the investigation of chemical and dynamical processes governing the upper atmosphere and ionosphere of Mars. These, in turn, offer insights to the escape rates of various atmospheric constituents.

[51] **Acknowledgments.** The authors would like to thank F. Forget and E. Millour for discussing the MCD, Y. Ma for sharing the Viking1 Lander RPA measurements, and L. Moore for insightful discussions of the hydrogen chemistry at Saturn. We also thank three anonymous reviewers for their constructive comments that improved the delivery of this study. This work was supported by grants from the NASA MDAP (NNX07AN99G) and MFRP (NNX08AN56G) programs.

References

- Anderson, D. E. (1974), Mariner 6, 7, and 9 ultraviolet spectrometer experiment: Analysis of hydrogen Lyman alpha data, *J. Geophys. Res.*, *79*, 1513–1518.
- Anderson, D. E., and C. W. Hord (1971), Mariner 6 and 7 ultraviolet spectrometer experiment: Analysis of hydrogen Lyman alpha, *J. Geophys. Res.*, *76*, 6666–6673.
- Anderson, D. E., and C. W. Hord (1972), Correction: “Mariner 6 and 7 ultraviolet spectrometer experiment: Analysis of hydrogen Lyman-alpha data” [J. Geophys. Res., Vol. 76, p. 6666–6673 (1971)], *J. Geophys. Res.*, *77*, 5638.
- Angelats i Coll, M., F. Forget, M. A. López-Valverde, F. González-Galindo (2005), The first Mars thermospheric general circulation model: the Martian atmosphere from the ground to 240 km, *Geophys. Res. Lett.*, *32*(4), L04201, doi:10.1002/jgra.50104.
- Anicich, V. (1993), A survey of bimolecular ion-molecule reactions for use in modeling the chemistry of planetary atmospheres, cometary comae, and interstellar clouds: 1993 supplement, *Astrophys. J.*, *84*, 215–315.
- Anicich, V. G., and W. T. Huntress (1986), A survey of bimolecular ion-molecule reactions for use in modeling the chemistry of planetary atmospheres, cometary comae, and interstellar clouds, *Astrophys. J. Suppl. Ser.*, *62*, 553–672.
- Banks, P., and G. Kockarts (1973), *Aeronomy*, Academic, San Diego, Calif.
- Barth, C. A., C. W. Hord, J. B. Pearce, K. K. Kelly, G. P. Anderson, and A. I. Stewart (1971), Mariner 6 and 7 ultraviolet spectrometer experiment: upper atmosphere data, *J. Geophys. Res.*, *76*, 2213–2227, doi:10.1029/JA076i010p02213.
- Barth, C. A., C. W. Hord, A. I. Stewart, and A. L. Lane (1972), Mariner 9 ultraviolet spectrometer experiment: initial results, *Science*, *175*(4019), 309–312.
- Bertaux J. L., and 26 co-authors (2000), The study of the Martian atmosphere from top to bottom with SPICAM light on Mars Express, *Pl. Sp. Sc.*, *18*, 1303–1320.
- Bougher, S. W., P.-L. Blelly, M. Combi, J. L. Fox, I. Mueller-Wodarg, A. Ridley, R. G. Roble (2008), Neutral upper atmosphere and ionosphere modeling, *Sp. Sc. Rev.*, *139*(1–4), 107–141.
- Chaufray, J. Y., R. Modolo, F. Leblanc, G. Chanteur, R. E. Johnson, J. G. Luhmann (2007), Mars solar wind interaction: formation of the Martian corona and atmospheric loss to space, *J. Geophys. Res.*, *112*, E09009, doi:10.1029/2007JE002915.
- Chaufray, J.-Y., J.-L. Bertaux, F. Leblanc, and E. Quémerais (2008), Observation of the hydrogen corona by SPICAM on Mars Express, *Icarus*, *195*, 598–613, doi:10.1016/j.icarus.2008.01.009.
- Chaufray, J. Y., F. Leblanc, E. Quémerais, and J. L. Bertaux (2009), Martian oxygen density at the exobase deduced from O I 130.4-nm observations by spectroscopy for the investigation of the characteristics of the atmosphere of Mars on Mars Express, *J. Geophys. Res.*, *114*, E02006, doi:10.1029/2008JE003130.
- Chen, R. H., and A. F. Nagy (1978), A comprehensive model of the Venus ionosphere, *J. Geophys. Res.*, *83*(A3), 1133–1140, doi:10.1029/JA083iA03p01133.
- Chen, R. H., T. E. Cravens, and A. F. Nagy (1978), The Martian ionosphere in light of the Viking observations, *J. Geophys. Res.*, *83*, 3871–3876.
- Cravens, T. E. (1987), Vibrationally excited molecular hydrogen in the upper atmosphere of Jupiter, *J. Geophys. Res.*, *92*, 11083–11100.
- Dementyeva, N. N., V. G. Kurt, A. S. Smirnov, L. G. Titarchuk, S. D. Chuvahin (1972), Preliminary results of measurements of UV emissions scattered in the Martian upper atmosphere, *Icarus*, *17*, 475–483.
- Feldman, P. D., et al. (2011), Rosetta-Alice observations of exospheric hydrogen and oxygen on Mars, *Icarus*, *214*(2), 394–399.
- Forget, F., F. Hourdin, R. Fournier, C. Hourdin, O. Talagrand, M. Collins, S. R. Lewis, P. L. Read, and J.-P. Huot (1999), Improved general circulation models of the Martian atmosphere from the surface to above 80 km, *J. Geophys. Res.*, *104*, 24155–24176.
- Fox, J. L. (2003), Effect of H_2 on the Martian ionosphere: implications for atmospheric evolution, *J. Geophys. Res.*, *108*(A6), 1223, doi:10.1029/2001JA000203.
- Fox, J. L. (2004a), Advances in the aeronomy of Venus and Mars, *Adv. Space Res.*, *33*, 132–139.
- Fox, J. L. (2004b), Response of the martian thermosphere/ionosphere to enhanced fluxes of solar soft X-rays, *J. Geophys. Res.*, *109*, A11310, doi:10.1029/2004JA010380.
- Fox, J. L. (2005), Effects of dissociative recombination on the composition of planetary atmospheres, *J. Phys. Conf. Ser.*, *4*, 32–37.
- Fox, J. L., and A. Dalgarno (1979), Ionization, luminosity and heating of the upper atmosphere of Mars, *J. Geophys. Res.*, *84*, 7315–7333, doi:10.1029/JA084iA12p07315.
- Fox, J. L., and F. M. Bakalian (2001), Photochemical escape of atomic carbon from Mars, *J. Geophys. Res.*, *106*, 28785–28795, doi:10.1029/2001JA000108.
- Fox, J. L., and K. E. Yeager (2006), Morphology of the near-terminator martian ionosphere: a comparison of models and data, *J. Geophys. Res.*, *111*, A10309, doi:10.1029/2006JA011697.
- Fox, J. L., and K. E. Yeager (2009), MGS electron density profiles: analysis of the peak magnitudes, *Icarus*, *200*, 2, 468–479.
- Fox, J. L., A. B. Hač (2009), Photochemical escape of oxygen from Mars: a comparison of the exobase approximation to a Monte Carlo method, *Icarus*, *204*, 2, 527–544.
- Fox, J. L., P. Zhou, and S. W. Bougher (1996), The Martian thermosphere/ionosphere at high and low solar activities, *Adv. Space Res.*, *17*, 203–218.
- Galli, A., P. Wurz, H. Lammer, H. I. M. Lichtenegger, R. Lundin, S. Barabash, A. Grigoriev, M. Holmström, H. Gunell (2006), The hydrogen exospheric density profile measured with ASPERA-3/NPD, *Sp. Sc. Rev.*, *126* (1–4), 447–467.
- González-Galindo, F., M. A. López-Valverde, M. Angelats i Coll, and F. Forget (2005), Extension of a Martian general circulation model to thermospheric altitudes: UV heating and photochemical models, *J. Geophys. Res.*, *110*, E09008, doi:10.1029/2004JE002312.
- González-Galindo, F., M. A. López-Valverde, G. Gilli, and F. Forget (2011), Study of the Martian ionosphere with a general circulation model, *The Fourth International Workshop on the Mars Atmosphere: Modeling and observation*, held 8–11 February, 2011, in Paris, France, Published online at <http://www-mars.lmd.jussieu.fr/paris2011/program.html>, pp.376–377.
- Gu, M. F. (2003), Dielectronic recombination rate coefficients for H-like through Ne-like isosequences of Mg, Si, S, Ar, Ca, Fe, and Ni, *Astrophys. J.*, *590*(2), 1131–1140.
- Haider, S. A., K. K. Mahajan, and E. Kallio (2011), Mars ionosphere: a review of experimental results and modeling studies, *Rev. Geophys.*, *49*, RG4001, doi:10.1029/2011RG000357.
- Hallett, J. T., D. E. Shemansky, and X. Liu (2005), A rotational-level hydrogen physical chemistry model for general astrophysical application, *Astrophys. J.*, *624*, 448–461.
- Hanson, W. B., S. Sanatani, and D. R. Zuccaro (1977), The Martian ionosphere as observed by the Viking retarding potential analyzers, *J. Geophys. Res.*, *82*, 4351–4363.
- Herd, C. R., N. G. Adams, and D. Smith (1990) OH production in the dissociative recombination of H_3O^+ , HCO^+ , and N_2OH^+ —Comparison with theory and interstellar implications, *Astrophys. J.*, *349*, 388–392.

- Huestis, D. L., et al. (2008), Cross sections and reaction rates for comparative planetary aeronomy, *Space Sci. Rev.*, *139*, 63–105, doi:10.1007/s11214-008-9383-7.
- Kaplan, Lewis D., G. Münch, and H. Spinrad (1964), An analysis of the spectrum of Mars, *Astrophys. J.*, *139*, 1–16.
- Kaplan, L. D., J. Connes, and P. Connes (1969), Carbon monoxide in the Martian atmosphere, *Astrophys. J.*, *157*, L187–L192.
- Kim, Y. H., and J. L. Fox (1994), The chemistry of hydrocarbon ions in the Jovian ionosphere, *Icarus*, *112*, 310–325.
- Kliore, A., D. L. Cain, G. S. Levy, V. R. Eshleman, G. Fjeldbo, and F. D. Drake (1965), Occultation experiment: results of the first direct measurement of Mars's atmosphere and ionosphere, *Science*, *149*(3689), 1243–1248.
- Kong, T. Y., and M. B. McElroy (1977), Photochemistry of the Martian atmosphere, *Icarus*, *32*, 168–189.
- Krasnopolsky, V. A. (1993a), Photochemistry of the Martian atmosphere (mean conditions), *Icarus*, *101*, 2, 313–332.
- Krasnopolsky, V. A. (1993b), Solar cycle variations of the hydrogen escape rate and the CO mixing ratio on Mars, *Icarus*, *101*, 1, 33–41.
- Krasnopolsky, V. A. (1995), Uniqueness of a solution of a steady state photochemical problem: applications to Mars, *J. Geophys. Res.*, *100*, E2, 3263–3276.
- Krasnopolsky, V. A. (2000), On the deuterium abundance on Mars and some related problems, *Icarus*, *148*(2), 597–602.
- Krasnopolsky, V. A. (2002), Mars' upper atmosphere and ionosphere at low, medium, and high solar activities: implications for evolution of water, *J. Geophys. Res.*, *107*, 5128, doi:10.1029/2001JE001809.
- Krasnopolsky, V. A. (2003), Spectroscopic mapping of Mars CO mixing ratio: detection of north-south asymmetry, *J. Geophys. Res.*, *108*(E2), 5010, doi:10.1029/2002JE001926.
- Krasnopolsky, V. A., and P. D. Feldman (2001), Detection of molecular hydrogen in the atmosphere of Mars, *Science*, *294*, 1914–1917.
- Krasnopolsky, V. A., M. J. Mumma, and G. R. Gladstone (1998), Detection of atomic deuterium in the upper atmosphere of Mars, *Science*, *280*, 1576–1580.
- Kuiper, G. P. (1952), *The Atmospheres of the Earth and Planets*, University of Chicago Press, Chicago.
- Lewis, S. R., M. Collins, P. L. Read, F. Forget, F. Hourdin, R. Fournier, C. Hourdin, O. Talagrand, and J.-P. Huot (1999), A climate database for Mars, *J. Geophys. Res.*, *104*, 24177–24194.
- Lichtenegger, H., H. Lammer, D. F. Vogl, S. J. Bauer (2004), Possible temperature effects of energetic neutral hydrogen atoms on the Martian exosphere, *Adv. Sp. Res.*, *33*(2), 140–144.
- Lichtenegger, H., H. Lammer, Y. Kulikov, S. Kazeminejad, G. Molina-Cuberos, R. Rodrigo, B. Kazeminejad, and G. Kirchengast (2006), Effects of low energetic neutral atoms on Martian and Venusian dayside exospheric temperature estimations, *Sp. Sc. Rev.*, *126*(1), 503–503.
- Liszt, H., R. Lucas and J. H. Black (2004), The abundance of HOC⁺ in diffuse clouds, *Astro. Astrophys.*, *428*, 117–120.
- Lollo A., P. Withers, K. Fallows, Z. Girazian, M. Matta, and P. C. Chamberlin (2012), Numerical simulations of the ionosphere of Mars during a solar flare, *J. Geophys. Res.*, *117*(A5), A05314, doi: 10.1029/2011JA017399.
- Martini, C. R., J. K. Wilson, and M. J. Mendillo (2003), Modeling day-to-day ionospheric variability on Mars, *J. Geophys. Res.*, *108*(A10), 1383, doi:10.1029/2003JA009973.
- McElroy, M. B., T. Y. Kong, and Y. L. Yung (1977), Photochemistry and evolution of the Mars' atmosphere: a Viking perspective, *J. Geophys. Res.*, *82*, 4379–4388.
- Mendillo, M., A. Lollo, P. Withers, M. Matta, M. Pätzold, and S. Tellmann (2011), Modeling Mars' ionosphere with constraints from same-day observations by Mars Global Surveyor and Mars Express, *J. Geophys. Res.*, *116*, A11303, doi:10.1029/2011JA016865.
- Millar, T. J., P. R. A. Farquhar, and K. Willacy (1997), The UMIST database for astrochemistry 1995, *Astron. Astrophys. Suppl. Ser.*, *121*, 139–185.
- Millour, E., et al. (2011), An improved Mars Climate database, *The Fourth International Workshop on the Mars Atmosphere: Modeling and observation*, held 8–11 February, 2011, in Paris, France, Published online at <http://www-mars.lmd.jussieu.fr/paris2011/program.html>, pp.268–271.
- Millward, G. H., R. J. Moffett, S. Quegan, and T. J. Fuller-Rowell (1996), A coupled thermosphere-ionosphere-plasmasphere model (CTIP), in *STEP: Handbook of Ionospheric Models*, ed. R. W. Schunk, p. 239–279.
- Mitchell, D. L., R. P. Lin, C. Mazelle, H. Rème, P. A. Cloutier, J. E. P. Connery, M. H. Acuña, and N. F. Ness (2001), Probing Mars' crustal magnetic field and ionosphere with the MGS Electron Reflectometer, *J. Geophys. Res.*, *106*, E10, 23,419–23,428.
- Mitchell, J. B. A., O. Novotny, J. L. LeGarrec, A. Florescue-Mitchell, C. Rebrion-Rowe, A. V. Stolyarov, M. S. Child, A. Svendsen, M. A. El Ghazaly, and L. H. Andersen (2005), Dissociative recombination of rare gas hydride ions: II. ArH⁺, *J. Phys B*, *38*(10), L175–L181.
- Moore, L., and M. Mendillo (2007), Are depletions in Saturn's ionosphere caused by explosive surges of water from Enceladus? *Geophys. Res. Lett.*, *34*, L12202, doi:10.1029/2007GL029381, 2007.
- Moore, L. E., M. Mendillo, I. C. F. Mueller-Wodarg, and D. L. Murr (2004), Modeling of global variations and ring shadowing in Saturn's ionosphere, *Icarus*, *172*, 503–520.
- Moore, L., I. Müller-Wodarg, M. Galand, A. Kliore, and M. Mendillo (2010), Latitudinal variations in Saturn's ionosphere: Cassini measurements and model comparisons, *J. Geophys. Res.*, *115*, A11317, doi:10.1029/2010JA015692.
- Moore, L., G. Fischer, I. Müller-Wodarg, M. Galand, and M. Mendillo (2012), Diurnal variation of electron density in the Saturn ionosphere: model comparisons with SEDs, *Icarus*, *221*, 508–516.
- Moos, H. W. (1974), An upper limit on H₂ ultraviolet emissions from the Martian exosphere, *J. Geophys. Res.*, *79*(19), 2887–2889, doi:10.1029/JA079i019p02887.
- Moses, J. I., and S. F. Bass (2000), The effects of external material on the chemistry and structure of Saturn's ionosphere, *J. Geophys. Res.*, *105*, 7013–7052.
- Mul, P. M., and J. W. McGowan (1979), Dissociative recombination of N₂H⁺ and N₂D⁺, *Ap. J.*, *227*, p. L157–L159.
- Müller-Wodarg, I. C. F., M. Mendillo, R. V. Yelle, and A. D. Aylward (2006), A global circulation model of Saturn's thermosphere, *Icarus*, *180*(1), 147–160.
- Nagy, A. F., A. J. Kliore, M. Mendillo, S. Miller, L. Moore, J. I. Moses, I. Mueller-Wodarg, and D. Shemansky (2009), Upper atmosphere and ionosphere of Saturn, *Saturn From Cassini-Huygens*, edited by M. K. Dougherty, L. W. Esposito, and S. M. Krimigis, pp. 181–202, Springer, New York.
- Nair, H., M. Allen, A. D. Anbar, Y. L. Yung, and T. R. Clancy (1994), A photochemical model of the Martian atmosphere, *Icarus*, *111*, 1, 124–150.
- Nier, A. O., and M. B. McElroy (1976), Structure of the neutral upper atmosphere of Mars—results from Viking 1 and Viking 2, *Science*, *194*, 1298–1300.
- Nier, A. O., W. B. Hanson, M. B. McElroy, A. Seiff, and N. W. Spencer (1972), Entry science experiments for Viking 1975, *Icarus*, *16*, 74–91.
- Nier, A. O., W. B. Hanson, A. Seiff, M. B. McElroy, N. W. Spencer, R. J. Duckett, T. C. D. Knight, and W. S. Cook (1976), Composition and structure of the Martian atmosphere: preliminary results from Viking 1, *Science*, *193*, 786–788.
- Nier, A. O., and M. B. McElroy (1977), Composition and structure of Mars' upper atmosphere—results from the neutral mass spectrometers on Viking 1 and 2, *J. Geophys. Res.*, *82*, 4341–4349.
- Nicholson, W. P., G. Gronoff, J. Liliensten, A. D. Aylward, and C. Simon (2009), A fast computation of the secondary ion production in the ionosphere of Mars, *Mon. Not. R. Astron. Soc.*, *400*, 369–382.
- Rosati, R. E., M. P. Skrzypkowski, R. Johnsen, and M. F. Golde (2007), Yield of excited CO molecules from dissociative recombination of HCO⁺ and HOC⁺ ions with electrons, *J. Chem. Phys.*, *126*(154302), doi: 10.1063/1.2715943.
- Schunk, R. W., and A. F. Nagy (2009), *Ionospheres*, 2nd ed. Cambridge University Press, New York.
- Scott, G. B., D. A. Fairley, C. G. Freeman, M. J. McEwan, P. Spanel, D. Smith (1997), Gas phase reactions of some positive ions with atomic and molecular hydrogen at 300 K, *J. Chem. Phys.*, *106*(10), 3982–3987.
- Singh, R. N., and R. Prasad (1983), Production of dayside ionosphere of Mars, *J. Astrophys. Astron.*, *4*, 261–269.
- Strickland, D. J., G. E. Thomas, and P. R. Sparks (1972), Mariner 6 and 7 ultraviolet spectrometer experiment: analysis of the O I 1304- and 1356-Å emissions, *J. Geophys. Res.*, *77*, 4052–4068.
- Tobiska, W. K. (2004), SOLAR2000 irradiances for climate change, aeronomy, and space systems engineering, *Adv. Space Res.*, *34*, 1736–1746.
- Vaille, A., V. Tenishev, M. Combi, S. Bougher, and A. Nagy (2009), Three-dimensional study of Mars upper thermosphere/ionosphere and hot oxygen corona: 1. General description and results at equinox for solar low conditions, *J. Geophys. Res.*, *114*, E11005, doi:10.1029/2009JE003388.
- Verner D. A., and D. G. Yakovlev (1995), Analytic FITS for partial photoionization cross sections, *Astron. Astrophys. Suppl.*, *109*, 125–133.
- Verner, D. A., G. J. Ferland, K. T. Korista, and D. G. Yakovlev (1996), Atomic data for astrophysics. II. New analytic fits for photoionization cross sections of atoms and ions, *Astrophys. J.*, *465*, 487–498.
- Withers, P. (2009), A review of observed variability in the dayside ionosphere of Mars, *Adv. Sp. Res.*, *44*, 3, 277–307.
- Young, L. D. G., and A. T. Young (1977), Interpretation of high-resolution spectra of Mars IV—new calculations of the CO abundance, *Icarus*, *30*, 75–79.